Journal of Power Sources 180 (2008) 15–22

Contents lists available at ScienceDirect

Journal of Power Sources

journal homepage: www.elsevier.com/locate/jpowsour

Evaluation of $Ba_{0.5}Sr_{0.5}Co_{0.8}Fe_{0.2}O_{3-\delta}$ as a potential cathode for an anode-supported proton-conducting solid-oxide fuel cell

Ye Lin [a], Ran Ran [a], Yao Zheng [a], Zongping Shao [a,*], Wanqin Jin [a], Nanping Xu [a], Jeongmin Ahn [b]

[a] State Key Laboratory of Materials-Oriented Chemical Engineering, Nanjing University of Technology, No. 5 Xin Mofan Road, Nanjing, JiangSu 210009, PR China
[b] School of Mechanical and Materials Engineering, Washington State University, Sloan 217, Pullman, WA 99164-2920, USA

ARTICLE INFO

Article history:
Received 23 January 2008
Received in revised form 20 February 2008
Accepted 20 February 2008
Available online 26 February 2008

Keywords:
Proton
Perovskite
Cathode
$Ba_{0.5}Sr_{0.5}Co_{0.8}Fe_{0.2}O_{3-\delta}$
Solid-oxide fuel cells

ABSTRACT

The potential application of $Ba_{0.5}Sr_{0.5}Co_{0.8}Fe_{0.2}O_{3-\delta}$ (BSCF) as a cathode for a proton-conducting solid-oxide fuel cell based on $BaCe_{0.9}Y_{0.1}O_{2.95}$ (BCY) electrolyte was investigated. Cation diffusion from BCY to BSCF with the formation of a perovskite-type Ba^{2+}-enriched BSCF and a Ba^{2+}-deficient BCY at a firing temperature as low as 900 °C was observed, the higher the firing temperature the larger deviation of the *A* to *B* ratio from unit for the perovskites. Symmetric cell tests demonstrated the impurity phases did not induce a significant change of the cathodic polarization resistance, however, the ohmic resistance of the cell increased obviously. Anode-supported cells with the electrolyte thickness of ~50 μm were successfully fabricated via a dual-dry pressing process for the single-cell test. Under optimized conditions, a maximum peak power density of ~550 and 100 mW cm^{-2} was achieved at 700 and 400 °C, respectively, for the cell with the BSCF cathode layer fired from 950 °C. At 500 °C, the ohmic resistance is still the main source of cell resistance. A further reduction in membrane thickness would envisage an increase in power density significantly.

1. Introduction

Solid-oxide fuel cells (SOFCs) are a promising clean power source characterized by high energy conversion efficiency, all solid cell components, high power density, low environmental impact and excellent fuel flexibility. Nowadays, there is increasing interest in SOFCs both for residential and stationary applications. Lowering the operating temperature of SOFCs from ~1000 to 400–800 °C can significantly improve materials' compatibility, reduce capital costs both for materials and operation, and prolong the operational lifetime. Typical SOFCs are based on oxygen-ion-conducting electrolyte (SOFC-O^{2-}) [1–3]. Recently, the proton-conducting SOFCs have also received considerable attention (SOFC-H^+) for reduced-temperature application [4–23]. Selected protonic conductors show even higher ionic conductivity than stabilized zirconia and doped ceria at <600 °C [20,24]. Furthermore, SOFC-H^+ have higher theoretical electromotive force (EMF) and electrical efficiency than SOFC-O^{2-} [25].

Although several oxides with high protonic conductivity at reduced temperature have been developed, the progress of SOFC-H^+ is much retarded as compared to SOFC-O^{2-}. Table 1 is a summary of the recent advances in the SOFC performance based on proton-conducting electrolyte in literature. Nowadays, peak power density of >1.0 W cm^{-2} at intermediate temperatures of 600–800 °C is frequently reported in literature for SOFC-O^{2-} with thin-film electrolytes [26–30], while the power density of SOFC-H^+ seldom exceeds 500 mW cm^{-2} [4–23].

In order to achieve high power density of SOFC-H^+ at reduced temperatures, besides the development of new electrolyte material with high protonic conductivity, the reduction of electrolyte thickness, the development of cathode with low over-potential is also of great importance. As compared to the great efforts in searching for new protonic oxides, the research on cathode for SOFC-H^+ is much less up to now. Uchida et al. have demonstrated that the cathodic overpotential of Pt in SOFC-H^+ could not be neglected below 800 °C [31]. Several authors have also exploited conducting oxides such as $La_{1-x}Sr_xMO_{3-\delta}$ (M = Co, Fe, Mn) as the cathode materials for SOFC-H^+ [32].

$Ba_{0.5}Sr_{0.5}Co_{0.8}Fe_{0.2}O_{3-\delta}$ (BSCF) is a mixed conductor with ultra-high oxygen ionic conductivity, which has demonstrated to be a high-performance cathode for SOFC based on oxygen-ion conducting electrolyte [26,27,33–36]. In this study the application of BSCF as a cathode for proton-conducting $BaCe_{0.9}Y_{0.1}O_{2.95}$ (BCY) electrolyte fuel cell was reported. The fuel cell performance was found to be closely related with the phase reaction between the cathode and the electrolyte layers. By optimizing the firing temperature, the fuel cells demonstrated high power density of >500 mW cm^2 at 700 °C and high OCV of ~1.06 V at 500 °C.

* Corresponding author. Tel.: +86 25 83587722; fax: +86 25 83365813.
E-mail address: shaozp@njut.edu.cn (Z. Shao).

0378-7753/$ – see front matter © 2008 Elsevier B.V. All rights reserved.
doi:10.1016/j.jpowsour.2008.02.044

Table 1
A summary of laboratory fuel cells based on proton-conducting electrolytes and their reported maximum power outputs (the precise stoichiometry of the compounds are not given)

Year	Fuel	Electrodes (anode/cathode)	Electrolyte thickness (μm)	Maximum power (mW cm^{-2})	T (°C)	Ref.
1988	H_2	Pt/Pt	Yb:$SrCeO_3$, 500	35	800	[4]
1990	H_2/CH_4/CH_3OH	Pt(Ni)/Pt	Nd:$BaCeO_3$, 500	150/125/100	1000	[5]
1991	H_2	Pt/Ag	Gd:$BaCeO_3$, 400	80	800	[6]
1992	H_2	Pt/Pt	Gd:$BaCeO_3$, 500	230	800	[7]
1993	H_2	Pt/Pt	Sm:$BaCeO_3$, 500	220	1000	[8]
1996	H_2	Pt/Pt	$BaCaNdO_9$, 1000	35	600	[9]
2002	H_2	Pd-loaded FeO/$BaPrCoO_3$	Y:$BaCeO_3$, 500	134	600	[10]
2003	H_2	Pt/Pt	Y:$BaZrCeO_3$, 500	30	800	[11]
2004	H_2	Pr-doped Y:$BaCeO_3$/$BaPrYO_3$	Pr-doped Y:$BaCeO_3$, 120	240	950	[12]
2004	4% H_2 in Ar	Pt/$LaCaFeCoO_3$	Gd:$BaCeO_3$, 1000	6	700	[13]
2005	H_2, NH_3	Pt/Pt	Gd:$BaCeO_3$, 1300	38/35	700	[14]
2005	H_2	Pd/unknown	Y:$BaCeO_3$, 0.7	1400	600	[15]
2006	H_2	Heat-treated $BaCeYO_3$/Pt	Y:$BaCeO_3$, 500	163	950	[16,17]
2006	H_2	Ni-$BaCeSmO_3$/$BaSrCoFeO_3$ + $BaCeSmO_3$	Sm:$BaCeO_3$, 50	340	700	[18]
2006	H_2, NH_3	Ni–$BaCeGdO_3$/$LaSrCoO_3$ + $BaCeGdO_3$	Gd:$BaCeO_3$, 50	371/355	700	[19]
2006	H_2	Ni/$BaCePrYO_3$	Y:$BaZrCeO_3$, 15	270	700	[20]
2007	H_2	Pt/Ag	Y:$BaCeO_3$, 500	18	500	[21]
2007	H_2, NH_3	Ni–$BaCeNdO_3$/$LaSrCoO_3$ + $BaCeNdO_3$	Nd:$BaCeO_3$, 20	335/315	700	[22]
2007	C_2H_6	Pt/Pt	Y:$BaCeO_3$, 800	120	700	[23]

2. Experimental

2.1. Synthesis of oxide power

Both BCY and BSCF powders were synthesized by a combined EDTA–citrate complexing sol–gel process [37,38]. The synthesis of BCY, as an example, is described as follows. Required amounts of analytic reagents of $Ba(NO_3)_2$, $Ce(NO_3)_3$, and $Y(NO_3)_2$, according to the cation stoichiometry of the composite oxide BCY, were prepared into a mixed solution under stirring. EDTA and citric acid were added to the solution at the mole ratio of total metal ions:EDTA:citric acid of 1:1:2. NH_4OH was applied to adjust the pH value of the solution to be around 6 during the water evaporation. Under stirring and heating, a clear viscous gel was obtained, which was solidified by pre-heating at 250 °C for several hours and finally calcined at 900–1100 °C for 5 h to obtain a pure-phase composite oxide with the nominated composition of BCY.

2.2. Cell fabrication

Symmetrical cells with the configuration of electrode|BCY|electrode were used for the impedance studies. Dense BCY pellets of 12 mm in diameter and 0.55 mm in thickness were prepared by die pressing and sintered in air at 1400 °C for 5 h. To prepare the electrode, the BSCF oxide powder was first prepared into a colloidal suspension by dispersing it into a mixed solution of glycerol, ethylene glycol and isopropyl alcohol by high-energy ball milling (Fritsch Pulverisettle 6) at the rotation rate of 400 rpm for 0.5 h. It was then spray-deposited symmetrically on both surfaces of the BCY pellets, followed by calcined at 950–1100 °C for 2 h in air. Silver paste was adopted as the current collectors.

Anode-supported cells with BCY electrolyte were prepared using a co-pressing technique. Anode powders were prepared by well mixing of NiO and BCY in weight ratio of 60 to 40 by a high-energy ball miller. To fabricate the single cell, the NiO + BCY powder was first pressed as a substrate, onto which the fine BCY powder was added and pressed again to form a bi-layer pellet. The electrolyte thickness was controlled by the amount of BCY applied during the fabrication. A final anode thickness of 0.56 mm was adopted. The green pellets were then sintered in air at 1400 °C for 5 h for the densification of the electrolyte layer, the diameter of the anode-supported cells is 13 mm. BSCF slurry was spray-deposited onto the central surface of the electrolyte and fired at various temperatures between 900 and 1100 °C in air for 2 h; the cathode effect area is ~0.26 cm^{-2} and its layer thickness is around 20 μm.

2.3. Electrochemical impedance test

The electrode performance was investigated with the symmetrical or complete cell configuration by the ac impedance method using an electrochemical workstation based on a Solartron 1260A frequency response analyzer in combination with a Solartron 1287 potentiostat. The frequency applied was ranged from 0.01 Hz to 1000 kHz with a signal amplitude of 30 mV under open cell voltage (OCV).

2.4. Single-cell test

The fuel cell reactor was put into a vertical split tube furnace, a thermocouple was inserted near the cathode surface both for the temperature controlling and monitoring. Three percent H_2O humidified H_2 at a flow rate of 80 ml min^{-1} [STP: standard temperature and pressure] was fed into the anode chamber as fuel while ambient air was applied as the cathode atmosphere. *I–V* polarization curves were collected using a Keithley 2420 source meter based on the four-probe configuration.

2.5. Other characterization

The phase structure of the oxides was examined by X-ray diffractometer (XRD, Bruker D8 Advance). The microscopic features of the prepared electrodes or single cell were characterized using an environmental scanning electron microscope (ESEM, QUANTA-2000). The powders were also conducted oxygen temperature-programmed desorption (O_2-TPD) experiment. About 150 mg of sample was loaded in a quartz tube, which was then placed in a single-zone furnace equipped with a temperature controller. Argon was used as the carrier gas with a flow rate of 20 ml min^{-1} [STP]. The temperature was increased from 50 to 950 °C at the rate of 10 °C min^{-1} and the effluent gases were monitored by the mass spectrometer (MS, Hiden, QIC-20).

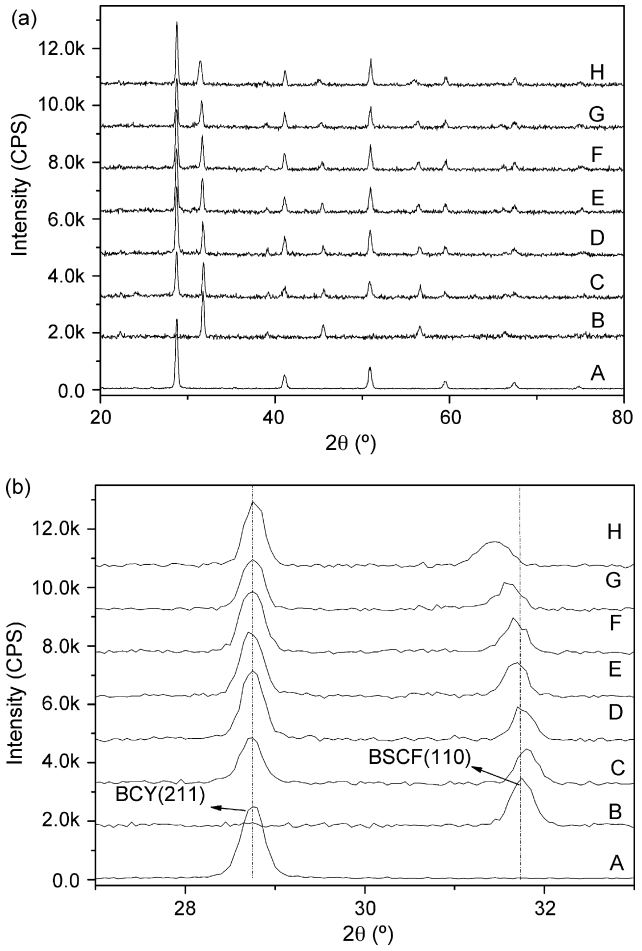

Fig. 1. X-ray diffraction patterns of: (A) pure BCY, (B) BSCF, (C) fresh mechanically mixed BSCF + BCY composite, (D–G) sample C further calcined/fired at 900, 950, 1000, 1050 and 1100 °C in air for 2 h, respectively.

3. Results and discussion

3.1. Phase reaction between BSCF and BCY

Interfacial phase reaction between fuel-cell components during the fuel-cell fabrication sometimes may become a practical problem. For example, it was found that the reaction between $La_{0.8}Sr_{0.2}MnO_{3-\delta}$ (cathode) and yttria-doped zirconia (electrolyte) was happened when the firing temperature for attaching the cathode layer to the electrolyte surface is 1100 °C or higher [39]. It led to the formation of non-conductive phases of $La_2Zr_2O_7$ and $SrZrO_3$ at the cathode–electrolyte interface, which significantly increased the interfacial polarization resistance of the cell and substantially deteriorated the fuel cell performance. BSCF is an active material, which has turned out to be reactive with samaria-doped ceria electrolyte at high temperatures [40]. To get the information about the possible phase formation at the cathode–electrolyte interface during the high-temperature firing, the solid-state reaction between BSCF and BCY was investigated by mixed powders. These two samples in powder state were mixed thoroughly at 1:1 weight ratio by high-energy ball milling for half hour and then calcined at various temperatures between 900 and 1100 °C for 2 h in air. The resulted products were then submitted to phase composition examination. Fig. 1A shows the room-temperature X-ray diffraction patterns of BSCF, BCY and the BSCF + BCY mixture after the calcinations at various temperatures. No other phase appeared even after the calcination at 1100 °C for 2 h. A more detailed observation of the diffraction patterns reveals that the diffraction peak of BSCF at mirror index of (1 1 0) shifted steadily to the lower 2θ direction with the increase of calcination temperature, while the diffraction peak of BCY perovskite at mirror index of (2 1 1) kept almost unmoved (Fig. 1B). Above phenomena strongly suggested that certain type of phase reaction between BSCF and BCY was actually happened during the high-temperature calcination, with the newly formed phases taking the same phase structure and similar lattice parameters to that of the reactants.

In a recent study, Tolchard and Grande reported the physiochemical compatibility of $SrCeO_3$ with $LaMO_3$ (M = Mn, Fe, Co) oxides, and they observed that the diffusion of Sr^{2+} in ceria is surprisingly fast with the primary reaction being the dissolution of SrO from $SrCeO_3$ into the $LaMO_3$, and corresponding formation of La-doped CeO_2 [41]. Similar phase reaction by cation exchange is likely happened between BSCF and BCY in our case. Four possibilities are available, (1) the exchange of Sr^{2+} in BSCF with Ba^{2+} in BCY with the formation of Ba^{2+}-enriched BSCF and Sr^{2+}-substituted BCY; (2) the exchange of B-site cation; (3) the diffusion of Ba^{2+} and Sr^{2+} from BSCF to BCY with the formation of A-site cation-deficient BSCF and Ba^{2+}-enriched BCY; and (4) the diffusion of Ba^{2+} from BCY to BSCF with the formation of A-site cation-enriched BSCF perovskite and Ba^{2+}-deficient BCY. Because Ba^{2+} (12-coordinated with oxygen, 1.61 Å) has larger ionic size than Sr^{2+} at the A-site (12-coordinated with oxygen, 1.44 Å) of perovskite, the cation exchange between Ba^{2+} in BCY with Sr^{2+} in BSCF would result in the lattice expansion of BSCF and the lattice shrinkage of BCY [42]. Since the lattice constant of BCY actually kept almost unchanged with respect to the firing temperature, the route (1) turns out to be unlikely, the route (2) is also less possible since the large difference in ionic radius between Ce^{4+}/Y^{3+} with Co^{3+}/Fe^{3+} in the B-site of perovskite. In our former studies [43,44], we have demonstrated that BSCF can still sustain its perovskite lattice structure over a large deviation of its A/B cation ratio from unit ($0.83 < A/B < 1.15$) while the lattice parameter increased and decreased, respectively, for the A-site cation enrichment and deficiency. On the other hand, Ma and Iwahara et al. have demonstrated that BCY can also tolerate a large deviation of its A/B ratio away from unit ($0.9 < A/B < 1.2$) [45], however its lattice constant kept almost unchanged no matter of either A-site cation deficiency or enrichment. Based on the results of Fig. 1, it is likely that the Ba^{2+} in BCY diffused to BSCF and resulted in the formation of Ba^{2+}-deficient BCY and A-site Ba^{2+}-enriched BSCF during the high temperature firing of BSCF + BCY mixture.

In a previous paper, we have demonstrated that O_2-TPD is an efficient and sensitive technique to characterize the local structural variation in BSCF [43]. Fig. 2 shows the O_2-TPD curves of BCY,

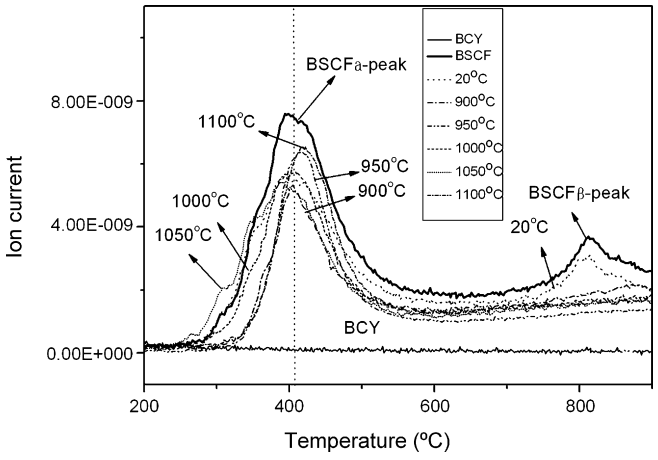

Fig. 2. O_2-TPD curves of BCY, BSCF and BSCF + BCY mixture before (20 °C) and after calcined at various temperatures (900–1100 °C) in air for 2 h.

BSCF and BSCF + BCY mixture after calcined at various temperatures in air for 2 h. BCY demonstrated no any oxygen desorption peak, it agrees well with no any multivalent metal ion available in its structure. BSCF demonstrated a big desorption peak at the intermediate-temperature range of 300–600 °C (α-peak) and a smaller desorption peak at 700–900 °C (β-peak), ascribed to the reduction of Co^{4+}/Fe^{4+} to Co^{3+}/Fe^{4+} and Co^{3+} to Co^{2+}, respectively [42]. It was observed that the β-peak disappeared after the high-temperature firing. Shao and coauthors have demonstrated that the cation enrichment at the A-site of BSCF resulted in the disappearance of high-temperature oxygen desorption peak [44], while the A-site cation deficiency resulted in increased intensity of the β-peak [43]. In another paper, Shao et al. have demonstrated that the β-peak could not be eliminated by varying the Ba^{2+} to Sr^{2+} ratio in the cation stoichiometric BSCF [42]. It then strongly supports that the reaction between BSCF and BCY is likely towards the formation A-site cation-enriched BSCF during the high-temperature firing.

3.2. Effect of interfacial reaction on the electrochemical performance

To evaluate the interfacial phase reaction between BSCF cathode and BCY electrolyte on their electrochemical performance, cells with thick BCY electrolyte and symmetrical BSCF electrodes were prepared. In order to create different degree of reaction at the interface between BSCF and BCY, various firing temperatures to fix the electrode layers onto the electrolyte surfaces were tried.

Fig. 3 shows the Nyquist plots of the electrochemical impedance spectra (EIS) of the various cells at 600 °C, with BSCF calcined between 900 and 1100 °C for 2 h. The high-frequency intercept of the impedance spectrum gives the ohmic resistance of the cell (R_{ohm}), which includes the resistive contributions of the electrolyte, the two electrodes, the current collectors and the lead wires, and also the interfacial layer of the reaction products (A-site cation-enriched BSCF and A-site cation-deficient BCY). In this study, the ohmic resistance of the two electrodes, the current collectors and the lead wires was reasonably considered to be negligible or the same for all samples. The low-frequency intercept gives the total resistance ($R_{ohm} + R_p$) of the cell, which includes the ohmic resistance of the cell, concentration polarization (mass-transfer or gas-diffusion polarization) resistance, and the polarization resistance associated with the electrochemical reactions at the electrode

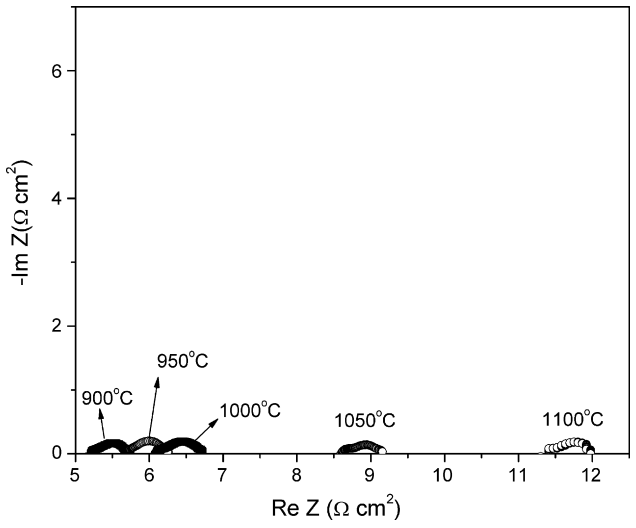

Fig. 3. Nyquist plots of the electrochemical impedance spectra (EIS) of the various symmetrical cells at 600 °C, with BSCF electrodes calcined between 900 and 1100 °C.

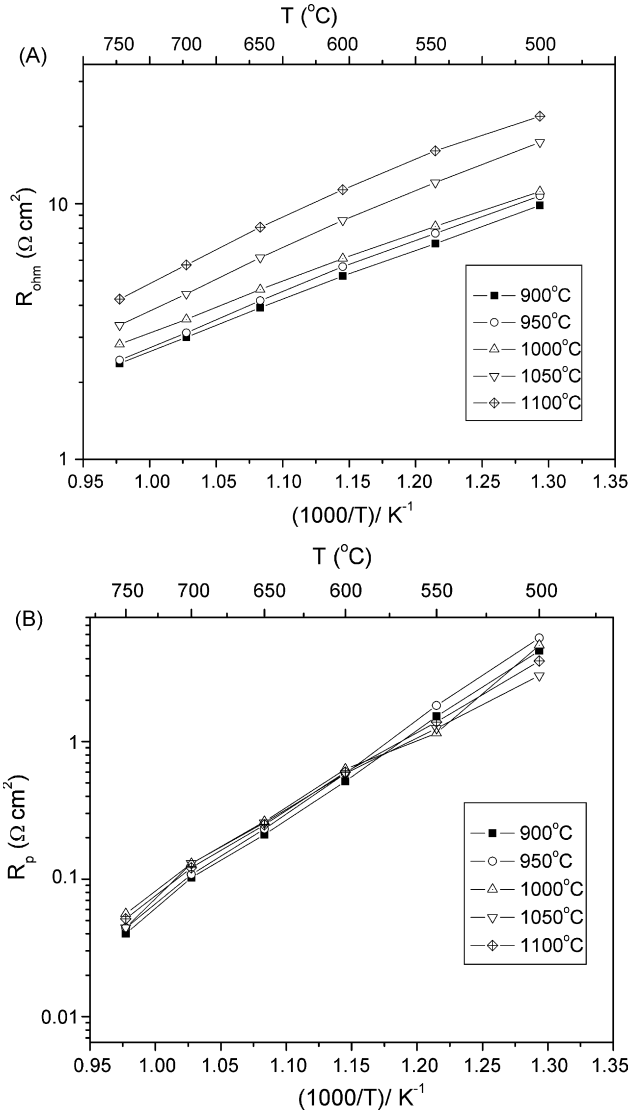

Fig. 4. Effect of firing temperature on: (A) the ohmic resistance (R_{ohm}) of BCY electrolyte (including the interfacial layer); (B) the area specific polarization resistance (R_p) of BSCF electrode based on symmetric cell configuration.

surface. As shown in Fig. 3, the ohmic resistance of the cell increased steadily with the temperature for firing the cathode layer to the electrolyte surface, while the polarization resistance did not change significantly.

Fig. 4A and B shows the temperature dependence of R_{ohm} and R_p, respectively. The ohmic resistance increased steadily with the firing temperature, and the increment in R_{ohm} is obvious at a firing temperature of 1050 °C or higher. Ma and Iwahara et al. have demonstrated that the A-site Ba^{2+}-enriched or A-site Ba^{2+}-deficient BCY could show significant lower protonic conductivity as compared to the cation stoichiometric BCY [45]. Based on the phase-reaction results of this study, the increase in the ohmic resistance with the firing temperature is attributed to the increase of A-site cation deficiency for the interfacial phase formed between BSCF and BCY. The conductivity of the electrolyte calculated based on the ohmic resistance in Fig. 4A is around 0.01 S cm^{-1} at 600 °C for the cell with cathode fired at 900 °C, which is comparable to the value (0.009 S cm^{-1}) reported by Ma and Iwahara et al. for a cation stoichiometric BCY [45]. It suggests that the impact of interfacial phase formation on the conductivity of thick BCY is not serious at

a firing temperature of 900 °C. In order to improve the cell performance, a decrease of the firing temperature for attaching the cathode layer to the electrolyte surface is then crucial. As compared to the ohmic resistance, the electrode polarization resistance was much less influenced by the firing temperature. The cells fired from 900 to 1000 °C show the lowest and highest area specific polarization resistances, respectively, at the operation temperature of 750 °C, while the 1050 °C calcined one shows the lowest and the 950 °C calcined one shows the highest at an operation temperature of 500 °C. As demonstrated in the previous section, the high-temperature firing resulted in the formation of an A-site Ba^{2+}-enriched BSCF. Zhou et al. have demonstrated that at small degree of cation enrichment, the A-site cation-enriched BSCF oxide shows even better electrode performance than the cation stoichiometric one [44]. On the other hand, the increase of firing temperature also resulted in the decrease of effective electrode surface area due to the cathode sintering. As a whole, no clear tendency of the cathodic polarization resistance with respect to the firing temperature was observed.

3.3. Anode-supported single cell fabrication and test

To evaluate the impact of the interfacial reaction between BSCF and BCY on the cathode performance of BSCF in a real fuel cell, or single cell with the configuration of (anode) BCY + NiO|thin-film BCY|BSCF (cathode) were constructed. Preparation of dense electrolyte membranes on porous anodes is an important step in the fabrication of high-performance SOFCs. Dual-dry pressing has tested to be a simple, reproducible and effective process for the preparation of anode-supported thin electrolyte dual-layer cell [46–48]. Several authors have also successfully reported the fabrication of supported thin-film protonic electrolyte by dual-dry pressing process [18–20]. In this study, the BCY + NiO anode-supported BCY dual-layer cells were also prepared by this technique. The thickness of the electrolyte was controlled by the amount of the electrolyte powder applied during the fabrication. The electrolyte layer is well densified and shows a main grain size of 1–2 μm (Fig. 5A). As shown in Fig. 5B, the electrolyte layer adhered to the anode surface pretty well, which ensures a low contacting

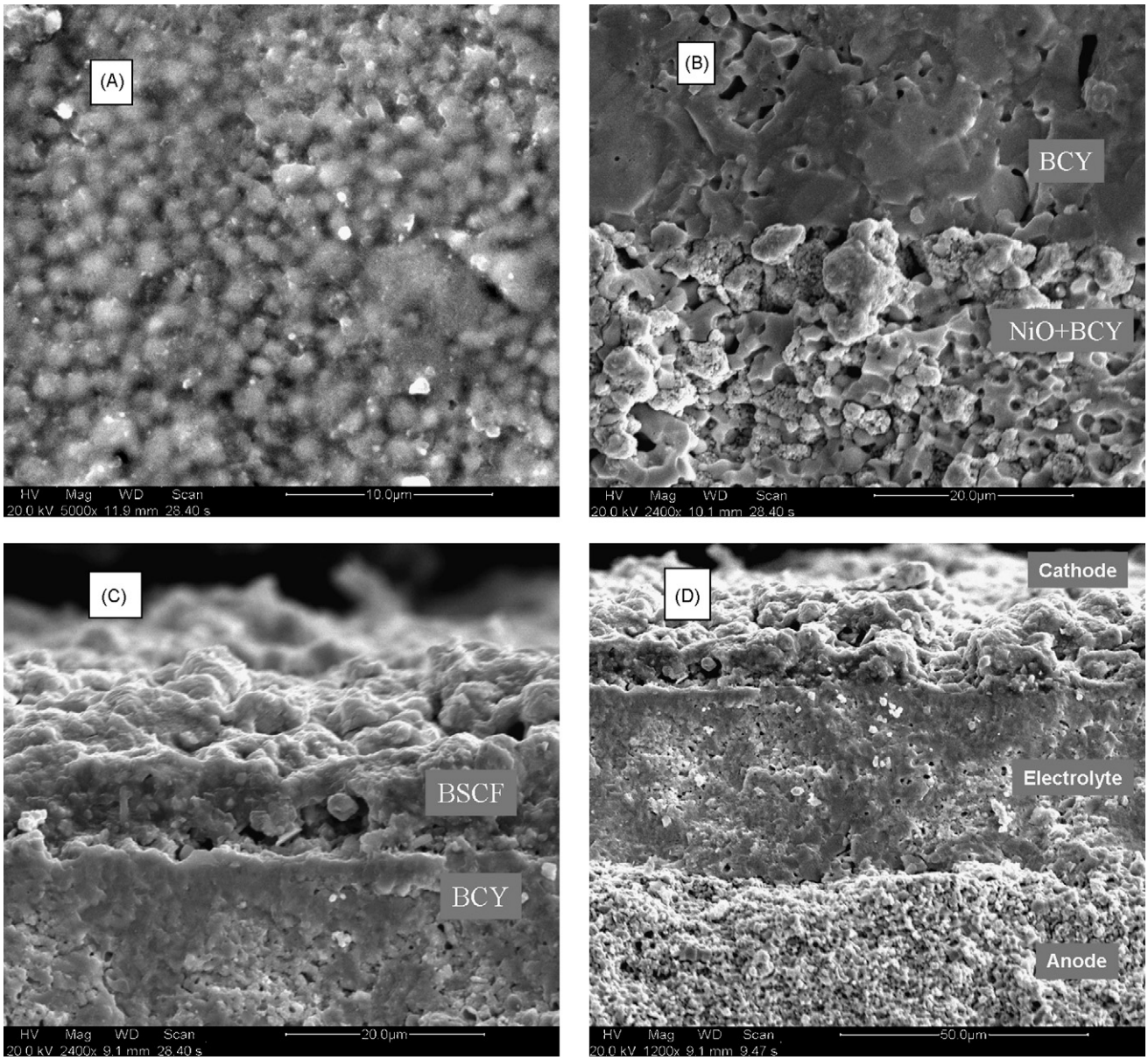

Fig. 5. SEM morphologies of: (A) BCY electrolyte surface; (B) cross-section of the 1400 °C calcined NiO + BCY supported BCY cell; (C) BSCF–BCY interface and (D) cross-section image of a post-examined single cell with reduced anode.

resistance between anode and electrolyte layer. The corresponding SEM images of the BSCF/BCY interface is shown in Fig. 5C, as we can see that there is no clear third layer appeared between BSCF and BCY layers. It suggests that the interface phase may be formed in a compositionally graded structure. We have tried the compositional analysis on the interface area by EDX method. However, due to the porous structure of the substrate the error is too large to get reasonable results. Definitively, it is worthwhile to find other method in our future work to clarify this issue. Fig. 5D shows the cross-section image of a post-examined single cell, the anode is highly porous and the fuel cell anode and cathode still adheres with the electrolyte layer pretty well.

Although a firing temperature of 900 °C has testified to result in the lowest degree of phase reaction between BSCF and BCY, as demonstrated by the symmetric cell test, the connection between cathode particles was relatively poor; therefore a firing temperature of 950 °C was applied for the single cell fabrication. For comparison, a firing temperature of 1100 °C was also conducted for the cathode layer. As shown in Fig. 6 are the SEM images of the cathodes fired at 950 and 1100 °C, respectively, the cathode fired at 1100 °C is much more sintered than that fired at 950 °C.

Single cells with anode thickness of ~600 μm, electrolyte of ~50 μm and cathode of ~20 μm were applied for the *I–V* polarization test. Fig. 7 shows the *I–V* curves of the single cells operated on pure hydrogen as the anode fuel and ambient air as the cathode oxidant. The linear response of cell voltage with respect to applied current, even at high current density, suggests that the concentration polarization did not occur for both cells. An attractive peak power density of ~550 mW cm^{-2} was achieved at an operation temperature of 700 °C for the cell with its cathode layer fired at 950 °C. It represents one of the highest power densities achieved for SOFC based on the proton-conducting oxide electrolyte, up to now. Even at an operation temperature of 400 °C, a peak power density of ~100 mW cm^{-2} was also reached. Furthermore, a high OCV of ~1.06 V was observed at 400 °C, suggesting that the electrolyte is sufficiently dense to prevent the gas leakage. As compared to the reduced-temperature SOFC-O^{2-}, the decrease in performance with respect to the reduction of temperature is much slower for the current proton-conducting SOFC [26]. It implies that SOFC-H^+ may be more suitable than SOFC-O^{2-} for low-temperature operation. As compared to the cell with the cathode fired from 950 °C, the cell with 1100 °C fired cathode shows much worse performance, as shown in Fig. 7B. A peak power density of only ~225 and ~60 mW cm^{-2} was achieved at an operation temperature of 700 and 400 °C, respectively, which is only about one half that of the cell with the cathode fired from 950 °C. Since this fuel cell also demonstrates high OCVs, the difference in their power densities is unlikely due to gas leakage.

As shown in Fig. 8 is the EIS of the single cells under OCV condition. The polarization resistances presented here are a sum of the cathode and anode polarization resistances. Very low area-specific polarization resistance of ~0.36 Ω cm^2 was observed at an operation temperature of 500 °C for the cell with cathode fired from 950 °C. It suggests that BSCF cathode performs pretty well with BCY electrolyte when the cathode was fired from 950 °C.

Fig. 9 shows the total cell resistance (R_{total}), electrode polarization resistance (R_p), cell ohmic resistance (R_{ohm}), and the ratio of ohmic resistance to cell resistance obtained from the impedance spectra at different temperatures. The ohmic resistance of the cell is still overwhelming at 500 °C. A reduction of the electrolyte thickness could then result in the increase of the cell performance significantly. As compared to the ohmic resistance, the polarization resistance of the cell increased only slightly with the firing temperature. For example, it is about 0.36 and 0.52 Ω cm^2 at 500 °C, respectively, for the cell with its cathode fired at 950 and 1100 °C. To ensure a reasonable comparison of the different cathodes via the single-cell test, the microstructure of the electrodes and the electrolyte were fabricated as identical as possible for different cells by strictly optimizing the fabrication technique, therefore, it is reasonable to assume the difference in area-specific polarization resistance of the cells was mainly contributed from the variation in cathode activity. Based on Fig. 6, such deterioration might be associated with the reduction of effective electrode surface area. However, the ohmic resistance of the cell increased more significantly from ~0.77 to ~1.39 Ω cm^2.

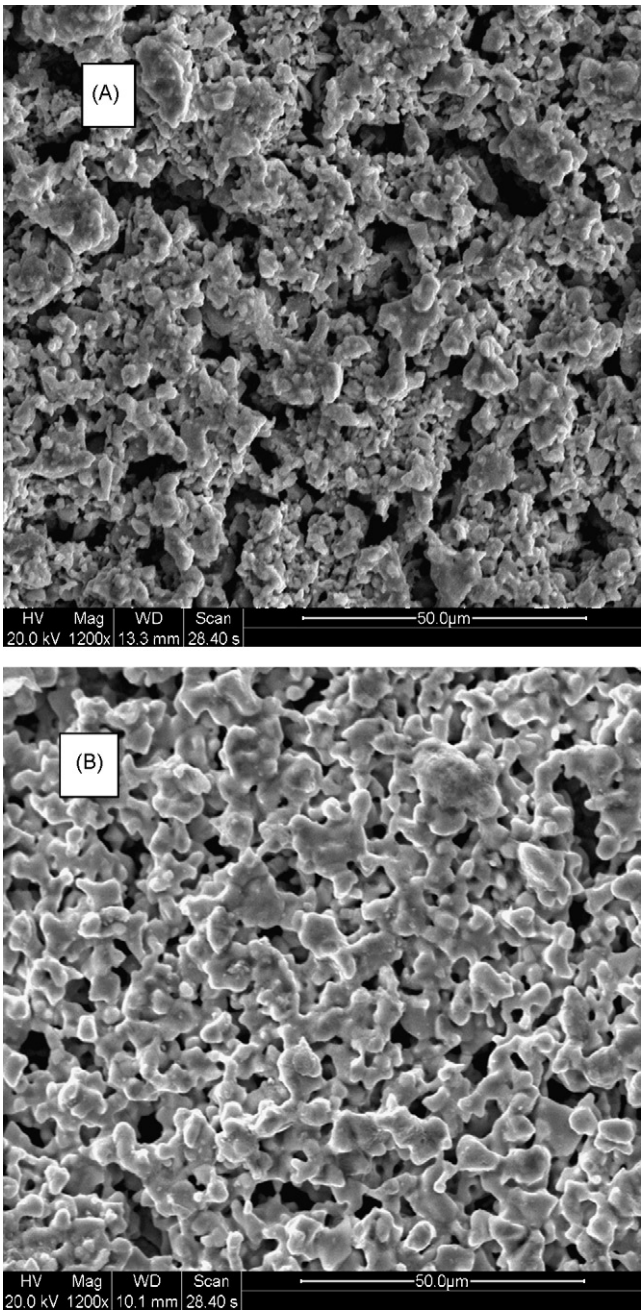

Fig. 6. SEM morphologies of the cathodes surface fired at: (A) 950 °C and (B) 1100 °C.

Fig. 10 shows the conductivities of the electrolyte layer (including the interfacial layer) of the cells with its cathode fired at 950 and 1100 °C, calculated based on the impedance data of the single cell under OCV condition, for comparison, the conductivities of the symmetric cells measured in dry air and with the electrode layer fired at 950 and 1100 °C, are also presented. For the asymmetric cell, a conductivity of ~0.0125, 0.0088, and 0.0065 S cm^{-1} was achieved,

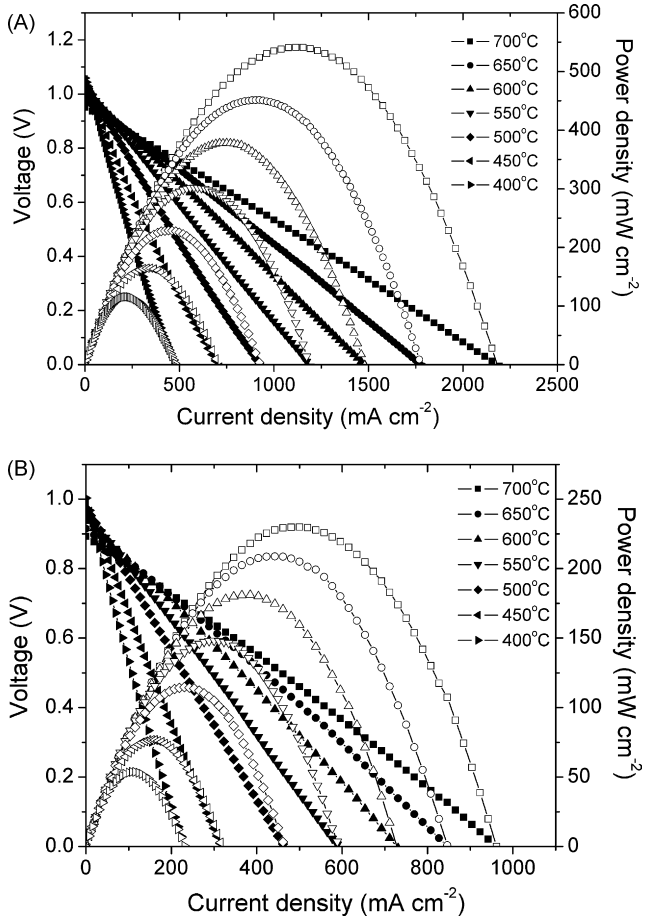

Fig. 7. The dependence of cell voltages and power densities on current densities of cell with 950 °C fired BSCF cathode layer (A), and 1100 °C fired BSCF layer (B), tested at various temperature between 400 and 700 °C.

respectively, at 700, 600 and 500 °C for the electrolyte (including the interfacial layer) with the cathode layer fired at 950 °C, while the conductivities decreased almost 50% for the electrolyte with the cathode fired at 1100 °C. It demonstrated that the formation of interfacial phase significantly blocked the protonic transportation from the electrolyte layer to the cathode layer, agreeing well with the results of the symmetric cell tests. It is reported that the protonic conductor usually shows smaller activation energy for proton conduction under hydrogen atmosphere than under air atmosphere [45]. Therefore, higher proton conductivity in air than in hydrogen is observed, respectively, at high temperature and low temperature zone. Higher conductivity of the electrolyte in the symmetric cell configuration (air/air) was observed at >600 °C than that in the asymmetric single cell configuration (air/H_2), agreeing with the literature results.

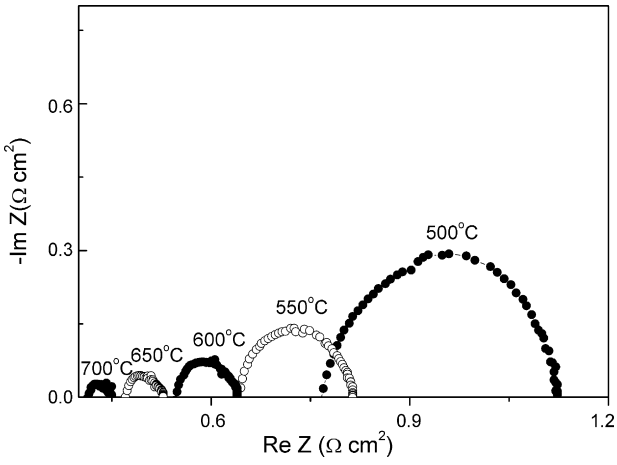

Fig. 8. EIS of the anode-supported fuel cell with 950 °C calcined BSCF at various temperatures under OCV conditions.

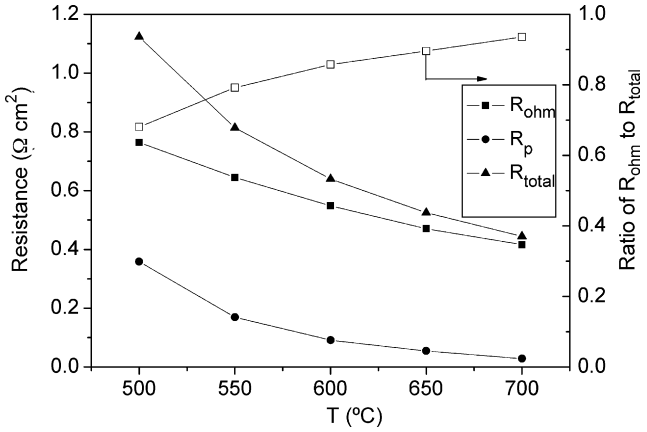

Fig. 9. The total cell resistances (R_{total}), interfacial polarization resistances (R_p), electrolyte resistances (R_{ohm}) and the ratio of electrolyte resistance to total resistance obtained from impedance spectra at different temperatures, of the cell with 950 °C fired BSCF cathode layer.

The only available data about BSCF cathode for proton-conducting electrolyte fuel cell is reported by Peng et al. [18]. They applied a BSCF + $BaCe_{0.9}Sm_{0.1}O_{2.95}$ (BCS) composite oxide as the cathode for a proton-conducting BCS electrolyte and a firing temperature of ~1100 °C for fixing the cathode layer to the electrolyte surface. An area-specific polarization resistance of ~2.25 Ω cm^2 was observed at 600 °C, which is significantly larger than our results. The electrode polarization resistance started to overwhelm the ohmic resistance at a temperature of 650 °C or lower. Their poor performance might be related with the high firing temperature (1100 °C) and the composite cathode applied. In the composite cathode, the A-site cation-deficient BCS was formed throughout the electrode layer, which could cover the BSCF surface and blocked the

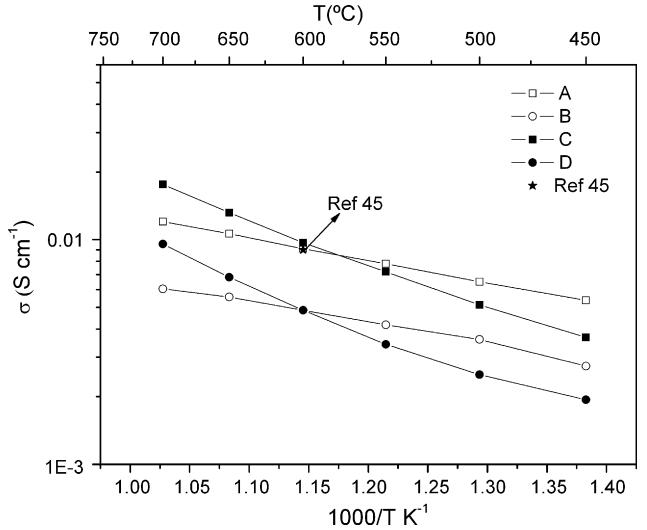

Fig. 10. Electrolyte (including the interfacial layer) conductivities obtained from the impedance data based on asymmetric single cell (H_2/air) with (A) 950 °C fired BSCF, (B) 1100 °C fired BSCF, and from symmetric cell in air with (C) 950 °C calcined BSCF, (D) 1100 °C fired BSCF cathode layer.

oxygen reduction over the cathode seriously. In our study, a pure BSCF was applied as the cathode layer, the phase reaction occurred only at the interface between BSCF cathode and BCY electrolyte. Therefore, the oxygen reduction properties of the cathode layer are not seriously affected.

4. Conclusions

The ohmic resistance of the cells (symmetric/asymmetric) based on BCY electrolyte and BSCF cathode seriously depends on the phase reaction between them, while the cathodic polarization resistance is not obviously impacted. The phase reaction involves the diffusion of Ba^{2+} from BCY electrolyte to the cathode and leads to the formation of Ba^{2+}-enriched BSCF and Ba^{2+}-deficient BCY interfacial phases, which have the same phase structure and similar lattice parameters to that of the reactants. Such impurity phases have small influence on the oxygen reduction kinetics over the cathode, however, they input a significant blocking effect on the proton transferring from electrolyte to the electrode. Therefore, an obvious increase of ohmic resistance of the cell was observed. The higher the firing temperature, the larger deviation of A/B ratio for the perovskites and the worse the cell performance, was observed. The optimal firing temperature is ~950 °C for the BSCF cathode layer. Anode-supported cell with electrolyte thickness of ~50 μm was successfully fabricated by a dual-dry pressing process. High performance of >500 mW cm^{-2} at 700 °C was reached for an anode-supported cell with the cathode layer fired from 950 °C, nearly twice that of the cell with cathode fired from 1100 °C. The results were attractive compared to the literature results. It suggests the potential application of BSCF as a cathode for SOFCs based on proton-conducting electrolytes. In order to further improve the cell performance, the reduction of electrolyte thickness and the prevention of the formation of Ba^{2+}-deficient BCY at the cathode–electrolyte interface is then of great importance, it will be our future research work on SOFC-H^+. On the other hand, composite cathode by mixing BSCF with electrolyte material may be not a good choice.

Acknowledgements

This work was supported by the National Natural Science Foundation of China under contract Nos. 20646002 and 20676061, National 863 Program under contract No. 2007AA05Z133, and National Basic Research Program of China under contract No. 2007CB209704.

References

[1] S.M. Haile, Acta Mater. 511 (2003) 5981–6000.
[2] R.M. Ormerod, Chem. Soc. Rev. 32 (2003) 17–28.
[3] S.P.S. Badwal, K. Foger, Ceram. Int. 22 (1996) 257–265.
[4] H. Iwahara, H. Uchida, K. Ogaki, J. Electrochem. Soc. 135 (1988) 529–533.
[5] H. Iwahara, H. Uchida, K. Morimoto, J. Electrochem. Soc. 137 (1990) 462–465.
[6] N. Bonanos, B. Ellis, M.N. Mahmood, Solid State Ionics 44 (1991) 305–311.
[7] N. Taniguchi, K. Hatoh, J. Niikura, T. Gamo, Solid State Ionics 53–56 (1992) 998–1003.
[8] H. Iwahara, T. Yajima, T. Hibino, H. Ushida, J. Electrochem. Soc. 140 (1993) 1687–1691.
[9] Y. Du, A.S. Nowick, Solid State Ionics 91 (1996) 85–91.
[10] T. Hibino, A. Hashimoto, M. Suzuki, M. Sano, J. Electrochem. Soc. 149 (2002) A1503–A1508.
[11] K.D. Kreuer, Annu. Rev. Mater. Res. 33 (2003) 333–359.
[12] D. Hirabayashi, A. Tomita, M.E. Brito, T. Hibino, U. Harada, M. Nagao, M. Sano, Solid State Ionics 168 (2004) 23–29.
[13] N. Maffei, L. Pelletier, A. Mctarlan, J. Power Sources 136 (2004) 24–29.
[14] N. Ito, M. Iijima, K. Kimura, S. Iguchi, J. Power Sources 152 (2005) 200–203.
[15] L. Pelletier, A. McFarlan, N. Maffei, J. Power Sources 145 (2005) 262–265.
[16] A. Tomita, T. Hibino, M. Sano, Electrochem. Solid-State Lett. 8 (2005) A333–A336.
[17] A. Tomita, K. Tsunekawa, T. Hibino, S. Teranishi, Y. Tachi, M. Sano, Solid State Ionics 177 (2006) 2951–2956.
[18] R.R. Peng, Y. Wu, L.Z. Yang, Z.Q. Mao, Solid State Ionics 177 (2006) 389–393.
[19] Q.L. Ma, R.R. Peng, Y.J. Lin, J.F. Gao, G.Y. Meng, J. Power Sources 161 (2006) 95–98.
[20] C.D. Zou, S.W. Zha, M.L. Liu, M. Hatano, M. Uchiyama, Adv. Mater. 18 (2006) 3318–3320.
[21] Y. Akimune, K. Matsuo, H. Higashiyama, K. Honda, M. Yamanaka, M. Uchiyama, M. Hatano, Solid State Ionics 178 (2007) 575–579.
[22] K. Xie, Q.L. Lin, Y.Z. Jiang, J.F. Gao, X.Q. Liu, G.Y. Meng, J. Power Sources 170 (2007) 38–41.
[23] S.Y. Wang, J.L. Luo, A.R. Sanger, K.T. Chuang, J. Phys. Chem. C 111 (2007) 5069–5074.
[24] W. Suksamai, I.S. Metcalfe, Solid State Ionics 178 (2007) 627–634.
[25] W. Amsak, S. Assabumrungrat, P.L. Douglas, N. Laosiripojana, S. Charojrochkul, Chem. Eng. J. 119 (2006) 11–18.
[26] Z.P. Shao, S.M. Haile, Nature 431 (2004) 170–173.
[27] Q.L. Liu, K.A. Khor, S.H. Chan, J. Power Sources 161 (2006) 123–128.
[28] S.D. Kim, H. Moon, S.H. Hyun, J. Moon, J. Kim, H.W. Lee, Solid State Ionics 178 (2007) 1304–1309.
[29] X.G. Zhang, M. Robertson, C. Decès-Petit, Y.S. Xie, R. Hui, S. Yick, E. Styles, J. Roller, O. Kesler, R. Maric, D. Ghosh, J. Power Sources 161 (2006) 301–307.
[30] T. Ishihara, J.W. Yan, M. Shinagawa, H. Matsumoto, Electrochim. Acta 52 (2006) 1645–1650.
[31] H. Uchida, S. Tanaka, H. Iwahara, J. Appl. Electrochem. 15 (1985) 93–97.
[32] H. Yamaura, T. Ikuta, H. Yahiro, G. Okada, Solid State Ionics 176 (2005) 269–274.
[33] J. Pena-Martinez, D. Marrero-Lopez, J.C. Ruiz-Morales, B.E. Buergler, P. Nunez, L.J. Gauckler, J. Power Sources 159 (2006) 914–921.
[34] J. Pena-Martinez, D. Marrero-Lopez, J.C. Ruiz-Morales, B.E. Buergler, P. Nunez, L.J. Gauckler, Solid State Ionics 177 (2006) 2143–2147.
[35] Y.S. Wang, S.R. Wang, Z.R. Wang, T.L. Wen, Z.Y. Wen, J. Alloys Compd. 428 (2007) 286–289.
[36] S. McIntosh, J.F. Vente, W.G. Haije, D.H.A. Blank, H.J.M. Bouwmeester, Chem. Mater. 18 (2006) 2187–2193.
[37] W. Zhou, Z.P. Shao, W.Q. Jin, J. Alloys compd. 426 (2006) 368–374.
[38] H.X. Gu, R. Ran, W. Zhou, Z.P. Shao, J. Power Sources 172 (2007) 704–712.
[39] A. Mitterdorfer, L.J. Gauckler, Solid State Ionics 111 (1998) 185–218.
[40] K. Wang, R. Ran, W. Zhou, H.X. Gu, Z.P. Shao, J. Ahn, J. Power Sources 179 (2008) 60–68.
[41] J. Tolchard, T. Grande, J. Solid State Chem. 180 (2007) 2808–2815.
[42] Z.P. Shao, G.X. Xiong, J.H. Tong, H. Dong, W.S. Yang, Sep. Purif. Technol. 25 (2001) 419–429.
[43] L. Ge, W. Zhou, R. Ran, S.M. Liu, Z.P. Shao, W.Q. Jin, N.P. Xu, J. Membr. Sci. 306 (2007) 318–328.
[44] W. Zhou, R. Ran, Z.P. Shao, W.Q. Jin, N.P. Xu, Acta Mater., doi:10.1016/j.actamat.2008.02.002, in press.
[45] G.L. Ma, T. Shimura, H. Iwahara, Solid State Ionics 110 (1998) 103–110.
[46] C.R. Xia, M.L. Liu, Solid State Ionics 144 (2001) 249–255.
[47] C.R. Xia, M.L. Liu, J. Am. Ceram. Soc. 84 (2001) 1903–1905.
[48] Z.P. Shao, C. Kwak, S.M. Haile, Solid State Ionics 175 (2004) 39–46.